High-resolution calorimetric study of the antiferroelectric liquid crystals methylheptyloxycarbonylphenyl octyloxybiphenyl carboxylate and its octylcarbonylbiphenyl analog

K. Ema and H. Yao
Department of Physics, Tokyo Institute of Technology, O-okayama, Meguro-ku, Tokyo 152, Japan

I. Kawamura
Showa Shell Sekiyu K. K., Central Research and Development Laboratory, 123-1 Shimokawairi, Atsugi, Kanagawa 243-02, Japan

T. Chan and C. W. Garland
Center for Materials Science and Engineering and Department of Chemistry, Massachusetts Institute of Technology, Cambridge, Massachusetts 02139
(Received 8 September 1992)

The antiferroelectric smectic-C^* (Sm-C^*) phases of two closely related chiral compounds have been studied with high-resolution calorimetric techniques. Both methylheptyloxycarbonylphenyl octyloxybiphenyl carboxylate (MHPOBC) and its octylcarbonylbiphenyl analog (MHPOCBC) exhibit Sm-C^*_α and Sm-C^*_A antiferroelectric phases. The Sm-A–Sm-C^*_α transitions are mean-field second order and well described by the usual extended Landau model. Three restructuring Sm-C^* transitions in MHPOBC studied with a relaxation calorimeter are shown to be sharp first-order transitions with very small latent heats. Pretransitional heat capacity associated with the Sm-C^*_A–Sm-I^*_A (hexatic smectic-I^*_A) transition and freezing of the monotropic Sm-C^*_A phase was studied in MHPOCBC.

PACS number(s): 64.70.Md, 61.30.−v, 64.60.Kw, 65.20.+w

I. INTRODUCTION

Since the first observation and initial characterization of antiferroelectricity in chiral liquid crystals [1–4], there has been a great deal of research on this subject. Much of this activity has focused on 4-(1-methylheptyloxycarbonyl)phenyl 4′octyloxy-biphenyl-4-carboxylate (MHPOBC), which exhibits ferroelectric and ferrielectric phases as well as two antiferroelectric smectic-C phases—Sm-C^*_α and Sm-C^*_A [5]. Recently, these Sm-C^*_α and Sm-C^*_A phases have also been observed in the closely related compound MHPOCBC, in which the octyloxy tail group is replaced by an octylcarbonyl group [6]. The structural formulas of these two compounds are

MHPOBC

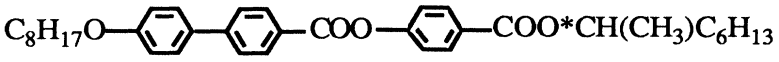

MHPOCBC

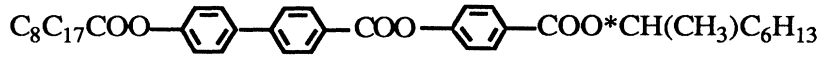

where * indicates the chiral center.

The sequence of phase transitions and the values of the transition temperatures in kelvin that have been reported for these compounds are

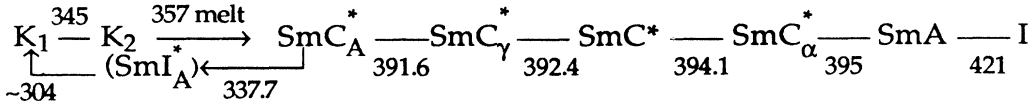

for MHPOBC (Refs. [3 and 5]) and

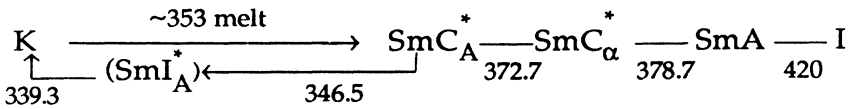

for MHPOCBC (Ref. [6]). The symbol K represents a crystal phase, I denotes the isotropic liquid crystal, and Sm-A is the smectic-A phase. There are four chiral smectic-C phases—ferroelectric Sm-C^*, ferrielectric Sm-C^*_γ, the two antiferroelectric phases Sm-C^*_α and Sm-C^*_A—and a chiral smectic-I (hexatic bond-orientational ordered) phase—Sm-I^*_A. Note that the Sm-I^*_A phases are monotropic. It will be shown below that these compounds freeze quite rapidly to the crystal near the Sm-C^*_A–Sm-I^*_A transition, and the temperature of the Sm-$C^*_A \rightarrow K$ transition depends strongly on the rate of cooling. The values quoted above were obtained from differential scanning calorimeter (DSC) measurements carried out at cooling rates of 1–5 K/min.

Reported in this paper are the results of high-resolution calorimetric studies of both MHPOBC and MHPOCBC. These include (1) an investigation of the second-order Sm-A–Sm-C^*_α transition in both materials, (2) a detailed study of the restructuring smectic-C^* transitions in MHPOBC, and (3) a study of the Sm-C^*_A–Sm-I^*_A pretransitional behavior and the kinetics of freezing in MHPOCBC. The experimental work on MHPOBC was carried out at the Tokyo Institute of Technology and that on MHPOCBC was carried out at the Massachusetts Institute of Technology. DSC measurements on both compounds were made at Showa Shell Sekiyu. Data analysis and the discussion of results is a joint effort.

II. EXPERIMENTAL RESULTS

High-purity (R)-MHPOBC and (R)-MHPOCBC samples were synthesized at Showa Shell Sekiyu, where R denotes the right-handed enantiomer. Commercially available (R)-2-octanol with an optical purity of 99% was used as the starting material, and it is expected that the optical purity of the MHPOBC and MHPOCBC is also about 99%. DSC measurements were carried out at Showa Shell using a Rigaku DSC-8240D instrument with a TAS-200 data analysis system. The details of the ac calorimeter used at MIT for the measurements on MHPOCBC have been described in Ref. [7]. The calorimeter used at TIT for the measurements on MHPOBC can be operated both in the ac mode and a relaxation mode, and details of its operation will be described elsewhere [8]. Basically, it has the same structure as the ac calorimeter at MIT, and the ac-mode operation is almost the same. The sample cell design has been modified slightly. Instead of using sample cells made of silver, a gold lid is pressed onto a gold cup without using tin or indium to improve the sample stability. In the relaxation mode, the power P supplied to the sample cell is a step function of time. In the heat regime, P is switched at time $t=0$ from 0 to a certain constant value P_0, or in the cool regime, from P_0 to 0. A standard calculation shows that the cell temperature relaxes exponentially to the equilibrium value

$$T(t)=T_B+T_\infty(1-e^{-t/\tau}) \quad (1)$$

for the heat regime, and

$$T(t)=T_B+T_\infty e^{-t/\tau} \quad (2)$$

for the cool regime. Here T_B is the bath temperature, $\tau=RC$, and $T_\infty=RP_0$, where C is the heat capacity of the sample cell and R is the thermal resistance between the cell and the bath. In the present measurement P_0 is 1.2 mW, and T_∞ is about 0.11 K. The heat capacity C is obtained by fitting the measured temperature response of the sample cell to Eqs. (1) and (2). In each measurement cycle in the relaxation mode, first the bath temperature is stabilized to a temperature which is 0.05 K higher (in a heating run) or lower (in a cooling run) than the previous setting. Then follows a pair of heat-regime and cool-regime measurements. The heat-regime comes first in heating runs, and the cool-regime comes first in cooling runs. The measurement cycle is repeated usually every 40 min. Therefore, the bath temperature is changed with an overall rate of 1.8 K/d. The MHPOBC sample was found to be fairly stable, with a T_c drift rate of about -0.02 K/d, which is much smaller than the above scan rate.

The C_p values determined in both the ac and the relaxation method were obtained from the following expression:

$$C_p=(C_p^{\text{obs}}-C_p^{\text{empty}})/m \ . \quad (3)$$

Here C_p^{obs} is the observed heat capacity of the filled cell, C_p^{empty} is the heat capacity of the empty cell, and m is the mass of the liquid-crystal sample in g.

A. MHPOBC results

Figure 1 shows an overview of C_p behavior observed for MHPOBC in the ac mode at 0.032 Hz on the first heating. The scan rate was around 1 K/h at all temperatures above 350 K. The sample melts into Sm-C^*_A phase at 356.9 K. The cusplike anomaly around 330 K may be ascribed to the phase transition between crystalline K_1 and K_2 phases. This anomaly was clearly seen only in the first heating run, and it became much smaller after the sample had been heated to above the melting temperature. A rather large discrepancy in the K_1-K_2 transition temperature between our value and the DSC result [3] ($\sim$345 K) is possibly due to the difference in scan rates. The scan rate used here was about 100 times slower than

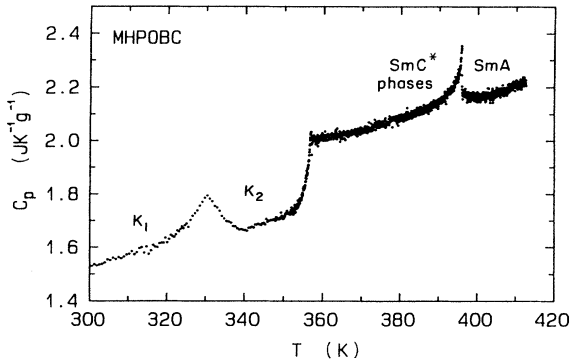

FIG. 1. Heat capacity of MHPOBC measured in the ac mode at 0.032 Hz. A detailed view of the Sm-C^*–Sm-A region is shown in Fig. 2.

the DSC scan rates.

Figure 2 is a detailed view of the C_p behavior in the Sm-C^*–Sm-A transition region. In agreement with the ac calorimeter results at 1 Hz by Chandani *et al.* [3], only the Sm-C^*_α–Sm-A transition peak is seen, and no features associated with Sm-C^*–Sm-C^* transitions are visible.

Figure 3 shows the C_p variation obtained in the relaxation mode for heat-regime relaxation measurements obtained during a heating run. Figure 3 is almost identical to the ac-mode result, except that there are three "odd" regions, shown by dashed arrows, where C_p has anomalously large values (see inset). The results shown in Figs. 2 and 3 were obtained on different samples, and a slight discrepancy in the C_p values is a reflection of the absolute accuracy of the present measurements, which is estimated to be about 10%. All three odd regions were seen in three different runs (runs *A*, *B*, and *C*) and their temperatures were quite reproducible. We call hereafter the three temperature regions where such odd heat capacities are seen region I, II, and III in order of increasing temperature.

To clarify the origin of such odd values of the heat capacity, the time response of the sample temperature was analyzed in detail. For this purpose, we define the time-dependence heat capacity as follows. Usually the heat capacity is given as the ratio of the heat absorbed by the sample to the increase in the sample temperature caused by the heat absorption,

$$C=\frac{\delta Q}{\delta T} . \tag{4}$$

We generalize this definition and define the $C(t)$, heat capacity at time t, as the ratio of the instantaneous heat flow into the sample cell $\dot{Q}$ to the instantaneous rate of its temperature change $\dot{T}$,

$$C(t)=\frac{\dot{Q}}{\dot{T}} . \tag{5}$$

This time-dependent heat capacity can be calculated from the measured time response of the sample temperature.

Figure 4(a) shows a typical plot of the time-dependent heat capacity, obtained for a measurement at 396.8 K,

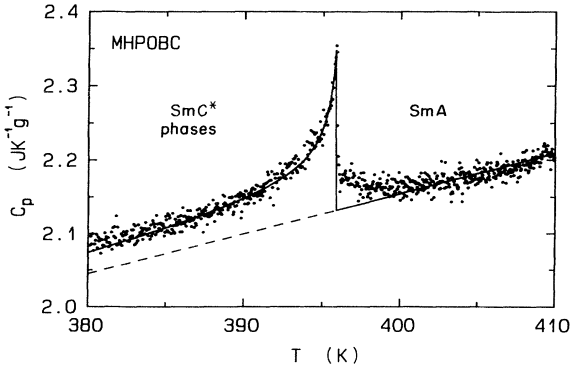

FIG. 2. Heat capacity of MHPOBC in the Sm-C^*–Sm-A region, measured in the ac mode at 0.032 Hz. The solid curve represents a Landau model fit with Eq. (8) and the dashed line shows the variation of $C_p^0(T)$ below T_c (see Sec. III A).

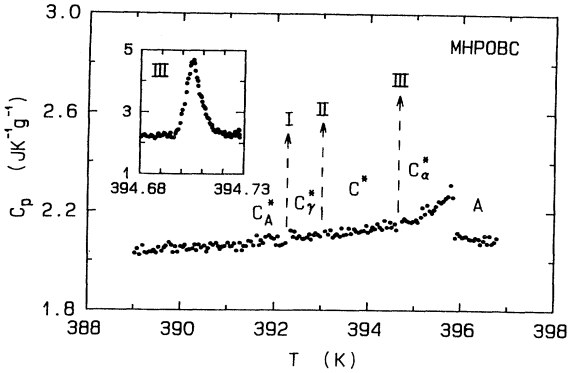

FIG. 3. Heat capacity of MHPOBC measured in the relaxation mode. Note that there are three anomalous regions indicated by the dashed arrows. The inset shows detailed *apparent* C_p values in region III; see the text.

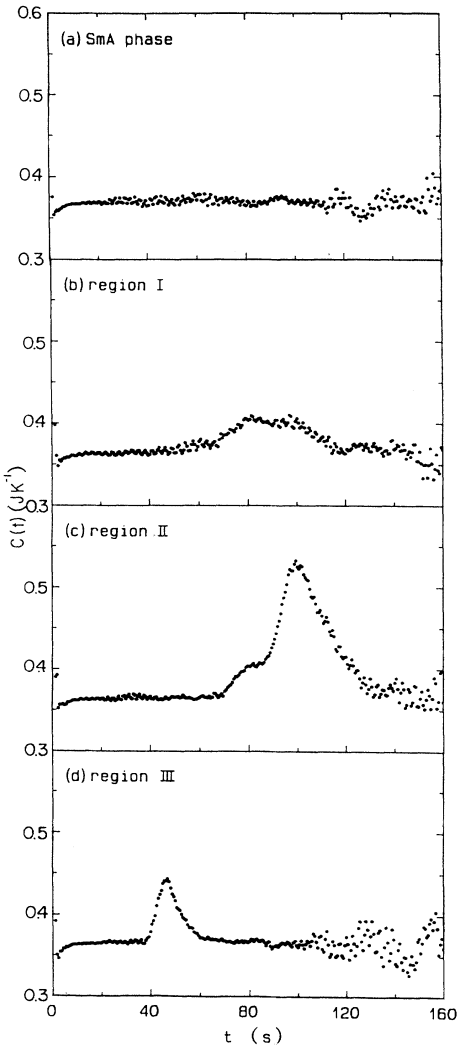

FIG. 4. Typical plots of the time-dependent MHPOBC heat capacity (a) obtained in run *A* at 396.8 K, (b) in run *C* in region I (Sm-C^*_A–Sm-C^*_γ), (c) in run *A* in region II (Sm-C^*_γ–Sm-C^*), and (d) run *A* in region III (Sm-C^*–Sm-C^*_α), where regions I–III represent the temperature regions where anomalies in the heat capacity are seen (see text).

TABLE I. Transition temperatures and thermal hystereses, in K, and the transition enthalpies for (*R*)-MHPOBC. Here T_c^H and T_c^C denote the transition temperatures on heating and cooling. The transition enthalpy for the Sm-C_α^*–Sm-A transition is not a latent heat but the total integrated enthalpy δH from 370 to 405 K (see Sec. III A).

			ΔH (J/mol)	
Transition	$\frac{1}{2}(T_c^H+T_c^C)$	$T_c^H-T_c^C$	ac relax.	DSC
Sm-C_α^*–Sm-A	395.9	0	370	165
Sm-C^*–Sm-C_α^*	394.6	0.05	12	9
Sm-C_γ^*–Sm-C^*	392.9	0.22	16	20
Sm-C_A^*–Sm-C_γ^*	392.3	0.18	9	4

which is in the Sm-A phase and away from any phase-transition temperature. This plot is essentially a flat straight line, showing that the heat capacity does not change as a function of time in this case. The larger scatter in data points in the large-t region is because both the denominator and the numerator of Eq. (5) approach zero, so that the experimental error in the ratio becomes relatively large. Figures 4(b)–4(d) show, on the other hand, typical plots of the time-dependent heat capacity obtained in the temperature regions I, II, and III. Distinct peaks are seen in all cases. The existence of such peaks in the time-dependent heat capacity means that extra heat is absorbed by the sample, and the most reasonable explanation is that it is caused by the absorption of the latent heat during a first-order phase transition.

Another support for the idea that the anomalies are caused by first-order phase transitions is the existence of thermal hystereses. Analyzing the data obtained in region III, we found that the anomaly occurs reproducibly with a thermal hysteresis of about 0.05 K. In temperature regions I and II, it was also found that the temperatures where the anomaly are seen show thermal hystereses.

From these experimental facts, we conclude that the three odd regions shown in Fig. 3 correspond to the three phase transitions between Sm-C^* phases: Sm-C_α^*–Sm-C^*, Sm-C^*–Sm-C_γ^*, and Sm-C_γ^*–Sm-C_A^*. A detailed view of the *apparent* heat capacity values obtained in one of these two-phase coexistence regions is shown as an inset in Fig. 3.

The value of the latent heat L is obtained by integrating the excess heat capacity

$$L=\int_0^\infty [C(t)-C_0]\dot{T}(t)dt \ . \tag{6}$$

Here C_0 is the normal time-independent value of the heat capacity, which is determined as the plateau value of $C(t)$ away from the transition region. Typical values of the transition temperatures, the thermal hystereses, and the transition enthalpies are summarized in Table I. The table also includes the transition enthalpies obtained by DSC measurements. Agreement between relaxation values and DSC values is quite good in view of the necessarily rapid DSC scan rates (3 K/min was used here).

B. MHPOCBC results

An overview of the C_p behavior observed for MHPOCBC over the 340–385 K range is shown in Fig. 5. The data below 355 K were obtained on cooling at a scan rate of 1 K/h = 17 mK/min. The Sm-C_α^*–Sm-C_A^* transition temperature and the K–Sm-C_A^* melting point on heating are marked by arrows in this figure. Note also the very sharp anomaly observed at 346 K, which represents a region of very rapid freezing as described below. Figure 6 shows C_p values obtained on heating at a scan rate of 1.5 K/h. This figure shows the large pretransitional heat capacity in the crystal K phase below the melting point at 353.4 K, as observed previously in other systems [9].

A detailed view of the C_p variation in the Sm-A–Sm-C_α^*–Sm-C_A^* region is shown in Fig. 7. The sample was quite stable, and the T_c drift rate was only −0.02 K/d. None of the ac calorimeter runs—heating or cooling—showed any thermal anomaly at the Sm-C_α^*–Sm-C_A^* transition. This is not surprising in view of the results on MHPOBC discussed in Sec. II A. Smectic-C restructuring transitions are first order with narrow coexistence ranges and very small latent heats. Furthermore, as discussed below in Sec. III, the integrated Sm-A–Sm-C^* enthalpy for MHPOCBC is much smaller than that for MHPOBC. Thus one might expect the Sm-C_α^*–Sm-C_A^* latent heat to be extremely small, and this is confirmed by a DSC value of 0.02 J g^{-1}. The fit to the Sm-A–Sm-C_α^* data with a mean-field Landau model is described in Sec. III A.

Several cooling runs in the region of the Sm-C_A^*–Sm-I_A^* transition of MHPOCBC are shown in Fig. 8. Above 349 K, the Sm-C_A^* phase is long-term metastable with respect to freezing. The values of $C_p(T)$ are reproducible on scanning T from ~370 K down to 349 K and then back up to 370 K. Furthermore, the C_p value at 349.3 K

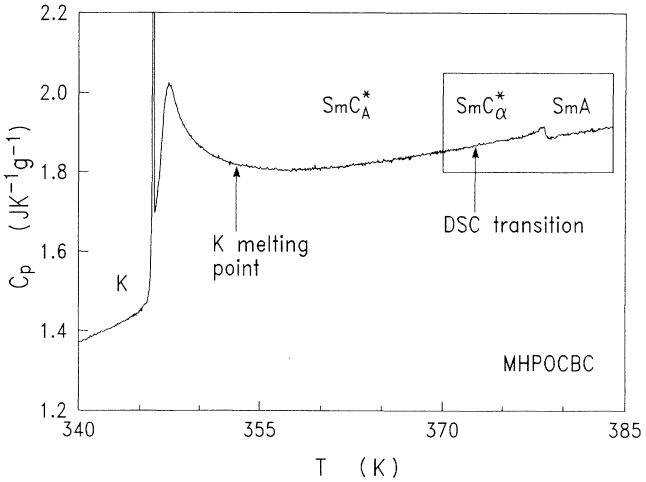

FIG. 5. Heat capacity of MHPOCBC. Data below 355 K were obtained on cooling at 1 K/h. The sharp spike at 346 K represents artificial C_p values, with associated anomalous phase shifts φ, in a region of rapid freezing. A detailed view of the Sm-A–Sm-C_α^* region enclosed in the box is shown in Fig. 7.

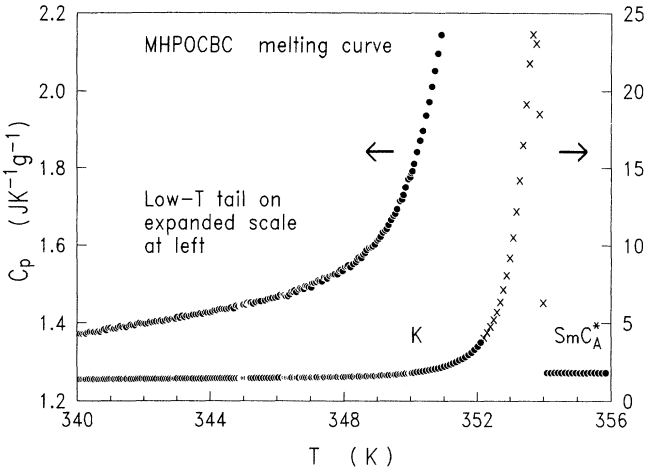

FIG. 6. Heat capacity of MHPOCBC obtained on heating. Pretransitional excess heat capacity occurs in phase K below the first-order melting transition at $T_1 = 353.4$ K. The K–Sm-C_A^* coexistence region is ~ 1.8 K wide, and points denoted by $\times$ are anomalous values obtained in this two-phase coexistence region.

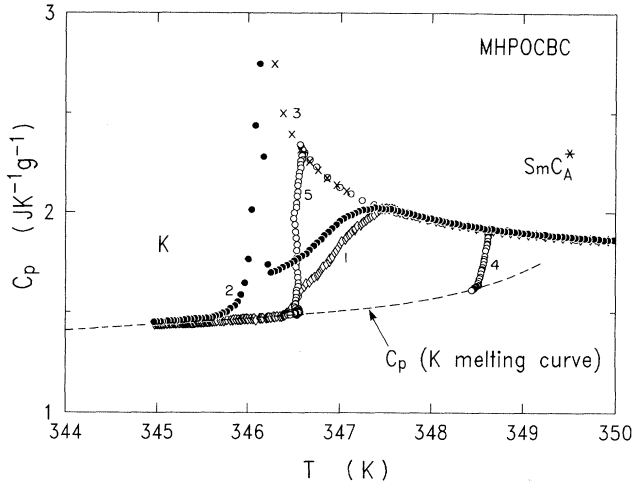

FIG. 8. Variation of C_p near the Sm-C_A^*–Sm-I_A^* transition in MHPOCBC. Below 349 K, the system freezes into crystal K at rates that are very sensitive to temperature. The dashed curve represents the C_p melting curve obtained when K is heated; see Fig. 6. Runs 1–3 were made at constant scan rates of -0.5, -1.0, and -4 K/h, respectively. Runs 4 and 5 were quench-and-hold runs with the temperature held approximately constant at 348.5–348.6 K and 346.5 K.

did not change when the sample was held at that temperature for 67 h. On cooling runs made at a constant scan rate, the data show evidence of slow freezing that begins around 347.5 K and terminates with a very rapid complete freezing at 346.0±0.2 K. Associated with the dramatic C_p spike at 346 K, there is an abrupt increase in the phase shift φ between the oscillating power input $\dot{Q}(\omega)$ and the resulting sample temperature oscillation $T_{ac}(\omega)$. These two features—artificially high values for the apparent C_p and a jump in φ values—are clear indications of two-phase coexistence [9,10]. Three constant-rate scans are shown in Fig. 8. Run 1 at -0.5 K/h exhibits a rounded C_p maximum at 347.5 K (indicating that slow freezing has begun to occur) and freezing is complete at 346.4 K 2 h later. Run 2 at -1 K/h exhibits a rounded maximum at 347.35 K and a sharp spike at 346.1 K. Run 3 at -4 K/h is so fast that no rounded C_p maximum can be resolved above 346 K, where a sharp freezing spike occurs (off the scale used in Fig. 3). Unfortunately, this run had to be terminated just below 346 K and no data are available at lower temperatures. Five other runs (not shown) with scan rates from -0.7 to -1.5 K/h confirm the general behavior shown for run 2.

In order to characterize the rate of freezing at constant

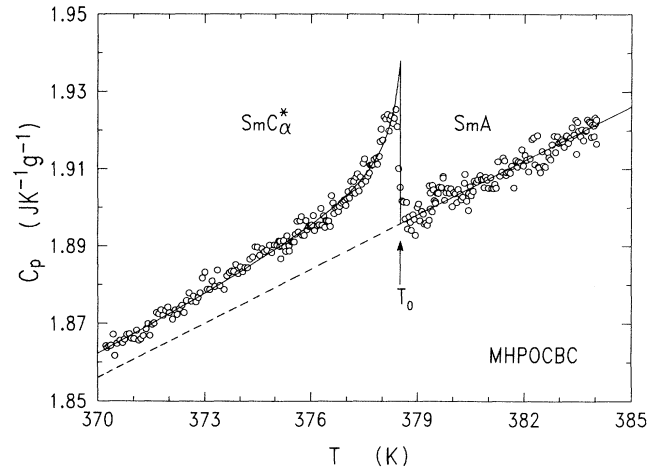

FIG. 7. Detail of the C_p variation near the Sm-A–Sm-C_α^* transition in MHPOCBC, measured in the ac mode. This run was obtained on heating, but equivalent results were also observed on cooling. The solid line represents a Landau model fit with Eq. (8) and the dashed line shows the variation of $C_p^0(T)$ below T_c.

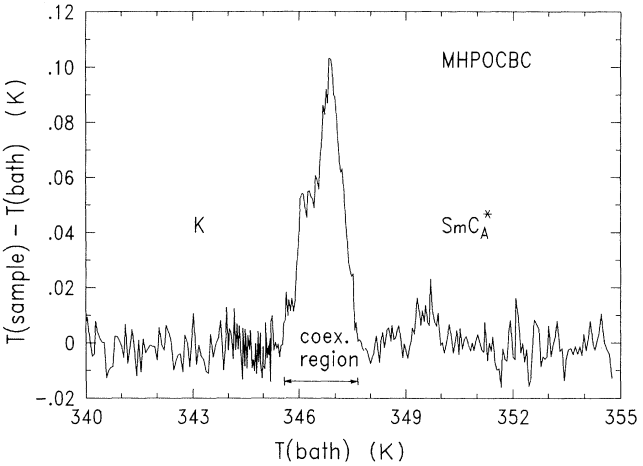

FIG. 9. Plot of [T(sample)$-T$(bath)] vs T(bath) for MHPOCBC cooling run 2 made at a scan rate of -1 K/h. The region where T(sample) is anomalously high corresponds to the liberation of latent heat during freezing.

TABLE II. DSC values of the transition enthalpies for (*R*)-MHPOCBC. These results were obtained on cooling at −3 K/min.

Transition	Order	DSC enthalpy (J/g)	DSC enthalpy (kJ/mol)
Sm-A–I	1st	10.1	5.95
Sm-C_α^*–Sm-A	2nd	0.10	0.060
Sm-C_A^*–Sm-C_α^*	1st	~0.02	~0.012
Sm-I_A^*–Sm-C_A^*	?	4.5–6.5	2.65–3.80
K–Sm-I_A^* (cooling)	1st	83.2	48.8
K–Sm-C_A^* (heating)	1st	100	58.7

temperature and the dependence of this rate on T, we carried out two more runs where the sample was cooled rapidly to a temperature below 349 K and then held at approximately constant temperature until freezing was complete. These "quench-and-hold" runs are shown in Fig. 8. Freezing into the crystal K phase required 7 h at $T_1 \cong 348.5$–348.6 K (run 4) and 2 h at $T_2 \cong 346.5$ K (run 5). From rapid constant-scan-rate runs, one can estimate that freezing occurs in $\lesssim 0.5$ h at 346 K. Also shown in Fig. 8 is a smooth dashed curve giving the variation of $C_p(T)$ for crystal K when it is heated. The data obtained on cooling runs agree very well with this curve after freezing is complete. Furthermore, C_p was also measured for several runs on heating *after* freezing was complete, and again the agreement (not shown) with the dashed curve is excellent.

As a confirmation that freezing is occurring during the waiting period of the quench-and-hold runs and also during constant-rate scans for temperatures below the value for the rounded C_p maximum, we compared the sample temperature with the bath temperature. When freezing occurs, the release of latent heat raises the sample temperature slightly above the expected value, as shown in Fig. 9. These results are completely consistent with the freezing behavior described above.

As a final point, we report the transition enthalpies for MHPOCBC determined from DSC measurements. These values are listed in Table II.

III. DISCUSSION

Our presentation of the discussion will be organized in three sections: the Sm-A–Sm-C_α^* transitions, the various Sm-C^* restructuring transitions in MHPOBC, and the Sm-C_A^* approach to Sm-I_A^* and subsequent freezing in MHPOCBC.

A. Sm-A–Sm-C_α^* transition

The Sm-A–Sm-C_α^* transitions are clearly mean field in character, as evidenced by the absence of appreciable excess heat capacity above the transition temperature T_c in both MHPOBC and MHPOCBC—see Figs. 2 and 7. These C_p data are well represented by the extended Landau model [11,12], for which the free energy has the form

$$G = G_0 + at\theta^2 + b\theta^4 + c\theta^6 , \tag{7}$$

where θ is the tilt order parameter and $t \equiv (T - T_c)/T_c$ is the reduced temperature. The resulting heat capacity expression is

$$C_p^+ = C_p^0(T) , \quad T > T_c , \tag{8a}$$

$$C_p^- = C_p^0(T) + A\frac{T}{T_c}\left[\frac{T_k - T_c}{T_k - T}\right]^{1/2} , \quad T < T_c , \tag{8b}$$

where $C_p^0(T) = B + E(T - T_c)$ is the regular background heat-capacity variation expected in the absence of a transition. The temperature T_k is a metastability limit, and the difference $T_k - T_c \equiv b^2 T_c/3ac$ is a measure of how far this second-order transition is from a classical tricritical point ($b = 0$ and thus $T_c = T_k$). Note that A is the magnitude of the discontinuous jump in C_p at the transition.

Fits with Eq. (8) are in good agreement with the experimental data, as shown in Figs. 2 and 7. The least-squares values of the fitting parameters are listed in Table III together with the integrated enthalpy δH defined by

$$\delta H = \int \Delta C_p dT , \tag{9}$$

where $\Delta C_p \equiv C_p - C_p^0$. The quantity δH can be evaluated from a numerical integration of the excess heat capacity or calculated from Landau theory using the parameter values obtained from the C_p fits with Eq. (8). The δH values in Table III are in reasonable agreement with the DSC values given in Tables I and II, but these high-resolution values are more accurate. It is also usual to quote the value of a quantity $t_0 \equiv 3(T_k - T_c)/T_c = b^2/ac$, since this determines the full width at half maximum of the C_p peak (i.e., $\Delta C_p = A/2$ at $t = -t_0$), and t_0 values are listed in Table III. It should be stressed that the shape of the fitting curve is very insensitive to T_c since $\Delta C_p \cong A^*(T_k - T)^{-1/2}$, where $A^* = (a^3/12cT_c)^{1/2} \cong (a^3/12cT_k)^{1/2}$; see Ref. [12]. The value of T_c is held fixed at the midpoint of the rapid rise in C_p at the transition.

Comparison of the Sm-A–Sm-C_α^* data and fit parame-

TABLE III. Landau parameters for fitting the Sm-A–Sm-C_α^* heat capacity data with Eq. (8). The units of A and B are $\mathrm{J\,K^{-1}\,g^{-1}}$. The values of background slope of E in units of $\mathrm{J\,K^{-2}\,g^{-1}}$ are $E = 0.0055$ for MHPOBC and $E = 0.0047$ for MHPOCBC. Also given are integrated enthalpies δH in both $\mathrm{J\,g^{-1}}$ and $\mathrm{J\,mol^{-1}}$ units and values of t_0.

System	T_c (K)	T_k (K)	B	A	$10^3 t_0$	δH (J/g)	δH (J/mol)
MHPOBC	395.92	396.170	2.132	0.243	1.92	0.66 ±0.07	370 ±40
MHPOCBC	378.50	378.708	1.896	0.042	1.65	0.11 ±0.01	65 ±6

ters for these two chiral compounds shows that the ΔC_p peak for MHPOCBC is much smaller than that for MHPOBC. In order to compare such nonuniversal amplitudes to those for other materials, it is best to convert the A values into dimensionless quantities $A_R = AM/R$, where M is the molecular weight in g (558.77 g for MHPOBC and 586.77 g for MHPOCBC). The resulting values are $A_R = 16.3$ for MHPOBC and $A_R = 3.0$ for MHPOCBC. For nonpolar nonchiral molecules, A_R and t_0 values range from $A_R = 5$, $t_0 = 6.5 \times 10^{-3}$ for $\overline{8}S5$ to $A_R = 47.8$, $t_0 = 0.8 \times 10^{-3}$ for 70.4 [11]. Larger A_R and smaller t_0 values have been reported for nonchiral molecules, but these were in systems close to tricritical or N-Sm-A-Sm-C^* multicritical points [13].

B. Various Sm-C^*-Sm-C^* transitions in MHPOBC

The phase transitions between Sm-C^* phases are detected only in the relaxation-mode measurement, and not in the ac method. From the relaxation-mode data, it is found that these phase transitions are sharp first-order ones with very narrow coexistence ranges, small thermal hystereses, and very small latent heats.

The temperature width of the coexistence region can be estimated from plots of the time-dependent heat capacity like those shown in Fig. 4. The smallest values of the coexistence widths obtained in several runs are 15 mK for Sm-C_A^*-Sm-C_γ^*, 13 mK for Sm-C_γ^*-Sm-C^*, and 4 mK for Sm-C^*-Sm-C_α^*. Furthermore, these estimated values actually give an upper limit in the sense that, if we could monitor the transition with a slower temperature scan rate, the temperature width might become even narrower.

As seen in Table I, the latent heats for the three Sm-C^*-Sm-C^* transitions are very small. There are at least two examples of phase transitions with similarly small latent heats: (A) the restacking transitions in the plastic crystal B phase of 70.7 [14], and (B) the lock-in transition in ferroelectric crystals of Rb_2ZnCl_4 group [15]. The former example involves transitions between crystal phases with different interlayer orderings [16]. In the latter case, there is a one-dimensional modulation in the displacement of atoms, and the period of the modulation shows a subtle change at the transition [15]. Therefore, both examples are quite similar to the present case of Sm-C^* transitions in MHPOBC in the sense that, in every case, there is only a rearrangement in the interlayer relationship at the phase transition, and the ordering within each layer remains essentially unchanged. It is also to be noted that measurements with an ac calorimeter failed to detect an anomaly at above-mentioned lock-in transitions [17,18].

C. Sm-C_A^*-Sm-I_A^* transition and freezing

As shown in Fig. 8, MHPOCBC exhibits pretransitional excess heat capacity on cooling that is associated with the approach to the Sm-C_A^*-Sm-I_A^* transition. However, on ac-calorimeter time scales, the sample freezes at or above this transition. (Since our calorimeter requires at least 3 min to measure C_p at each point, meaningful data cannot be obtained at scan rates greater than ~4 K/h, which is 50–100 times slower than typical DSC scans.) A comparison between our MHPOCBC data and C_p data for racemic methylbutylphenyloctyloxybiphenyl carboxylate (8*OSI*) is given in Fig. 10(a). 8*OSI* is a chiral compound that exhibits stable hexatic Sm-I and plastic crystal Cr-J phases [19]. Furthermore, the integrated enthalpy δH(8*OSI*) for the Sm-C-Sm-I transition is 4.2 J g^{-1}, in reasonably good agreement with the DSC enthalpy for MHPOCBC.

Figure 10(a) shows that the size and shape of the MHPOCBC C_p wing exactly matches that for 8*OSI* if one shifts the origins of the T and C_p scales without changing the scale sizes. Furthermore, the sharp spike in the heat capacity of MHPOCBC at 346.0 K corresponds to the position of C_p(max) in 8*OSI*, which is the effective

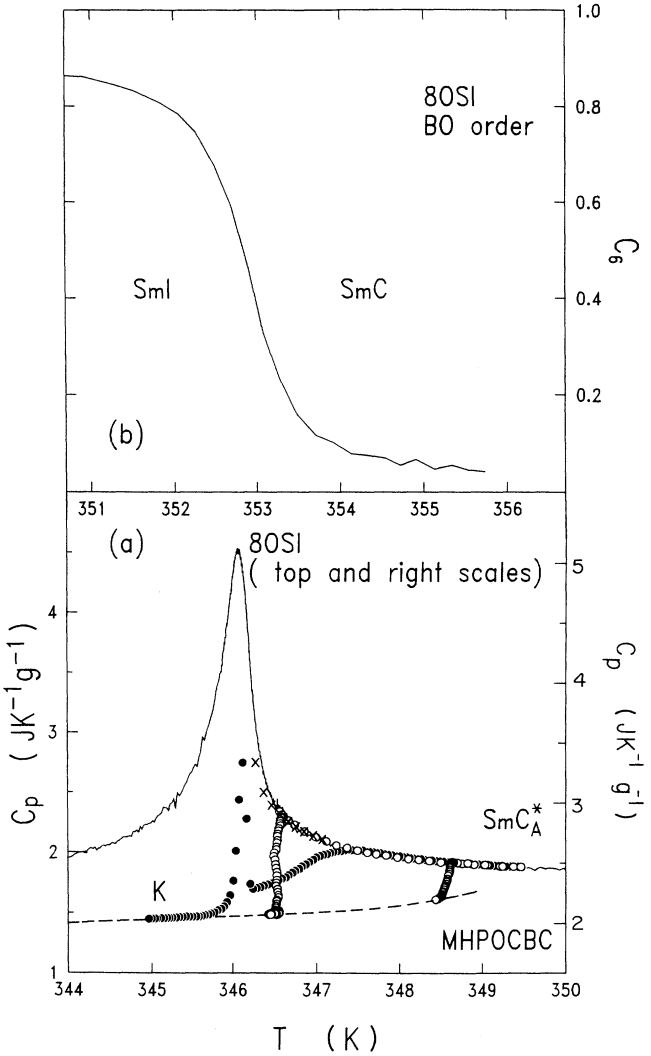

FIG. 10. (a) Comparison of Sm-C-Sm-I heat capacity variation for 8*OSI* (Ref. [19]) with MHPOCBC data from runs 2–5. Note that the sharp C_p spike at 346 K corresponds to the position of the transition temperature in 8*OSI*. (b) Bond-orientational order C_6 for 8*OSI*.

Sm-C–Sm-I transition temperature. The variation of the long-range bond-orientational hexatic order parameter C_6 is shown in Fig. 10(b). Due to the presence of a finite tilt field, there is long-range order *above* the effective transition temperature [19]. Let us assume that $C_6(T)$ for MHPOCBC is similar to that shown for 8*OSI*. Thus, we would expect $C_6 \simeq 0.04$ at 349 K rising to $C_6 \simeq 0.23$ at 346.5 K and $C_6 \simeq 0.54$ at "T_c"$=346$ K. These values are based on the hypothesis that in the absence of freezing MHPOCBC would undergo a continuous supercritical evolution of bond-orientational order like 8*OSI* and not a discontinuous first-order Sm-C_A^*–Sm-I_A^* transition.

We propose that the Sm-C_A^* phase does not freeze easily to crystal K for moderate ranges of supercooling. However, it seems reasonable that the bond-orientationally ordered Sm-I_A^* phase can freeze much more easily since only translational lock-in is required. The equilibrium freezing point of MHPOCBC is 353.4 K. In the range 349 K down to 346.5 K, the extent of C_6 ordering is rather fragmentary, and freezing proceeds only gradually. But when T approaches 346 K, C_6 increases dramatically, and the rate of freezing does so also. The pretranslational Sm-C_A^*–Sm-I_A^* wing is not seen in high-resolution studies of MHPOBC, since the extent of supercooling is much greater: $T_{\text{melt}} - T_{CI} = 19$ K, in contrast to 7.5 K for MHPOCBC.

Although our measurements were not designed to characterize the freezing kinetics, it is possible to obtain a preliminary view of this interesting feature. The fraction $X(t)$ crystallized at a given time t after a quench can be estimated from $C_p(t) = XC_p(K) + (1-X)C_p(\text{Sm-}C^*)$, where $C_p(K)$ is given by the dashed line in Fig. 10(a). For a two-dimensional Avrami model of nucleation and growth [20], which is appropriate for the freezing of a smectic liquid crystal, one has $X = 1 - \exp[-A(t)]$, where

$$A(t) = fG_xG_y\dot{N}_0 \int_0^t (t-\tau)^2 e^{-\nu\tau} d\tau \ . \tag{10}$$

G_x and G_y are linear growth rates, f is a geometric shape factor, $\dot{N} = \dot{N}_0 e^{-\nu\tau}$ is the two-dimensional (2D) nucleation rate (number of nuclei formed per unit area per sec) that decays with time, and τ is an incubation time. For $\nu t \gg 1$ (long times, associated with slow growth), $A(t) \simeq (f/\nu)G_xG_y\dot{N}_0 t^2$; and for $\nu t \ll 1$ (the regime probed when the growth is rapid), $A(t) \simeq (f/3)G_xG_y\dot{N}_0 t^3$. In these limits, one can write $A(t) = B_n t^n$, which leads to

$$\log_{10}\left[\ln\frac{1}{(1-X)}\right] = \log_{10} A(t) = n \log_{10} t + \log_{10} B_n \ . \tag{11}$$

Thus a log-log plot of $\ln(1-x)^{-1}$ vs t should yield a limiting slope of $n=3$ at short times, curving down to a final limiting slope $n=2$ at long times. Such plots of our data over the most reliable range $0.15 < X(t) < 0.95$ are curved for run 4 at early times and yield $n \simeq 2$ at later times and are quite straight, yielding $n \simeq 3$ for run 5. This trend toward the homogeneous nucleation limit for the rapidly freezing system is just what one would expect, and agrees with a study of the freezing of 40.8 from Sm-A to a plastic crystal B phase [21].

IV. CONCLUSION

The antiferroelectric Sm-C^* phases of MHPOBC and MHPOCBC have been studied with high-resolution calorimetric techniques. The Sm-C_α^*–Sm-A transitions were well described by the usual extended Landau model. The relaxation-mode measurements on MHPOBC revealed that three restructuring Sm-C^* transitions in this material are sharp first-order ones with very narrow coexistence ranges, small thermal hystereses, and very small latent heats. No thermal anomalies were detected at these restructuring Sm-C^* transitions with the ac method for either of the materials. The Sm-C_A^* phase of MHPOCBC freezes above the Sm-C_A^*–Sm-I_A^* transition with strongly temperature-dependent kinetics.

ACKNOWLEDGMENTS

The work at TIT was partly supported by a Grant-in-Aid for Scientific Research (No. 02640253) from the Ministry of Education, Science and Culture. The work at MIT was supported by National Science Foundation Grant No. DMR-90-22933. The authors wish to thank Dr. T. Hagiwara and Mr. H. Suzuki for experimental assistance with synthesis and DSC analysis and Professor Atsuo Fukuda and Professor Hideo Takezoe for stimulating and helpful discussions.

[1] A. D. L. Chandani, T. Hagiwara, Y. Suzuki, Y. Ouchi, H. Takezoe, and A. Fukuda, Jpn. J. Appl. Phys. **27**, L729 (1988).

[2] M. Fukui, H. Orihara, Y. Yamada, N. Yamamoto, and Y. Ishibashi, Jpn. J. Appl. Phys. **28**, L849 (1989).

[3] A. D. L. Chandani, Y. Ouchi, H. Takezoe, A. Fukuda, K. Terashima, K. Furukawa, and A. Kishi, Jpn. J. Appl. Phys. **28**, L1261 (1989).

[4] A. D. L. Chandani, E. Gorecka, Y. Ouchi, H. Takezoe, and A. Fukuda, Jpn. J. Appl. Phys. **28**, L1265 (1989).

[5] Y. Takanishi, K. Hiraoka, V. K. Agrawal, H. Takezoe, A. Fukuda, and M. Matsushita, Jpn. J. Appl. Phys. **30**, 2023 (1991); K. Hiraoka, Y. Takanishi, K. Skarp, H. Takezoe, and A. Fukuda, *ibid.* **30**, L1819 (1991).

[6] T. Isozaki, Y. Suzuki, I. Kawamura, K. Mori, N. Yamamoto, Y. Yamada, H. Orihara, and Y. Ishibashi, Jpn. J. Appl. Phys. **30**, L1573 (1991); T. Isozaki, K. Hiraoka, Y. Takanishi, H. Takezoe, A. Fukuda, Y. Suzuki, and I. Kawamura, Liq. Cryst. **12**, 59 (1992).

[7] C. W. Garland, Thermochim. Acta **88**, 127 (1985).

[8] K. Ema, T. Uematsu, A. Sugata, and H. Yao (unpublished).

[9] K. J. Lushington, G. B. Kasting, and C. W. Garland, J. Phys. Lett. (Paris) **41**, L419 (1980).

[10] K. Ema, G. Nounesis, C. W. Garland, and R. Shashidhar, Phys. Rev. A **39**, 2599 (1988).

[11] C. C. Huang and J. M. Viner, Phys. Rev. A **25**, 3385 (1982); see also M. Meichle and C. W. Garland, *ibid.* **27**, 2624 (1983), and references cited therein.
[12] C. W. Garland and M. E. Huster, Phys. Rev. A **35**, 2365 (1987).
[13] J. Boerio-Goates, C. W. Garland, and R. Shashidhar, Phys. Rev. A **41**, 3192 (1990); X. Wen, C. W. Garland, and M. D. Wand, *ibid.* **42**, 6087 (1990).
[14] J. Thoen and G. Seynhaeve, Mol. Cryst. Liq. Cryst. **127**, 229 (1985).
[15] K. Nomoto, T. Atake, B. C. Chaudhuri, and H. Chihara, J. Phys. Soc. Jpn. **52**, 3475 (1983), and references cited therein.
[16] J. Collett, L. B. Sorensen, P. S. Pershan, J. D. Litster, R. J. Birgeneau, and J. Als-Nielsen, Phys. Rev. Lett. **49**, 553 (1982).
[17] K. Hamano, Y. Ikeda, T. Fujimoto, K. Ema, and S. Hirotsu, J. Phys. Soc. Jpn. **49**, 2278 (1980).
[18] K. Ema, H. Saito, and K. Hamano (unpublished).
[19] C. W. Garland, J. D. Litster, and K. J. Stine, Mol. Cryst. Liq. Cryst. **170**, 71 (1989).
[20] J. E. Burke and D. Turnbull, Prog. Met. Phys. **3**, 220 (1952); H. Orihara, Y. Ishibashi, and Y. Yamada, J. Phys. Soc. Jpn. **57**, 4101 (1988).
[21] P. Oswald and F. Melo, J. Phys. II France **2**, 1345 (1992).